THE EUROPEAN
PHYSICAL JOURNAL C

Regular Article - Theoretical Physics

Bottomonia production and polarization in the NRQCD with k_T-factorization. II: $\Upsilon(2S)$ and $\chi_b(2P)$ mesons

N. A. Abdulov[1,2]**, A. V. Lipatov**[2,3,a]

[1] Faculty of Physics, Lomonosov Moscow State University, Moscow 119991, Russia
[2] Skobeltsyn Institute of Nuclear Physics, Lomonosov Moscow State University, Moscow 119991, Russia
[3] Joint Institute for Nuclear Research, Dubna, Moscow Region 141980, Russia

Abstract The $\Upsilon(2S)$ production and polarization at high energies is studied in the framework of k_T-factorization approach. Our consideration is based on the non-relativistic QCD formalism for bound states formation and off-shell production amplitudes for hard partonic subprocesses. The direct production mechanism, feed-down contributions from radiative $\chi_b(3P)$ and $\chi_b(2P)$ decays and contributions from $\Upsilon(3S)$ decays are taken into account. The transverse momentum dependent gluon densities in a proton were derived from the Ciafaloni–Catani–Fiorani–Marchesini evolution equation, Kimber-Martin-Ryskin prescription and Parton Branching method. Treating the non-perturbative color octet transitions in terms of the mulitpole radiation theory, we extract the corresponding non-perturbative matrix elements for $\Upsilon(2S)$ and $\chi_b(2P)$ mesons from a combined fit to $\Upsilon(2S)$ transverse momenta distributions measured by the CMS and ATLAS Collaborations at the LHC energies $\sqrt{s} = 7$ and 13 TeV and from the relative production rate $R_{\Upsilon(2S)}^{\chi_b(2P)}$ measured by the LHCb Collaboration at $\sqrt{s} = 7$ and 8 TeV. Then we apply the extracted values to investigate the polarization parameters λ_θ, λ_ϕ and $\lambda_{\theta\phi}$, which determine the $\Upsilon(2S)$ spin density matrix. Our predictions have a good agreement with the currently available data within the theoretical and experimental uncertainties.

1 Introduction

Since it was first observed, the production of charmonia and bottomonia in hadronic collisions remains a subject of considerable theoretical and experimental studies [1–16]. The theoretical framework for the description of heavy quarkonia production and decays provided by the non-relativistic QCD (NRQCD) factorization [17,18]. This formalism implies a separation of perturbatively calculated short-distance cross-sections for the production of $Q\bar{Q}$ pair in an intermediate Fock state $^{2S+1}L_J^{(a)}$ with spin S, orbital angular momentum L, total angular momentum J and color representation a from long-distance non-perturbative matrix elements (NMEs), which describe the transition of that intermediate $Q\bar{Q}$ state into a physical quarkonium via soft gluon radiation.

However, NRQCD meets some difficulties in simultaneous description of the charmonia and bottomonia production cross section and polarization data, as we have explained in our previous paper [19]. So, for example, having the NMEs fixed from fitting the charmonia transverse momentum distributions, one disagrees with the polarization observables: if the dominant contribution comes from the gluon fragmentation into an octet $Q\bar{Q}$ pair, the outgoing meson must have strong transverse polarization. The latter disagrees with the latest data [20–24], which show the unpolarized or even longitudinally polarized particles (so called "the polarization puzzle"). Moreover, the NMEs, obtained from the collider data, dramatically depend on the minimal transverse momentum used in the fits [25] and are incompatible with each other when obtained from fitting the different data sets.

A potential solution to this problem was proposed [26] in the framework of a model that interprets the soft final state gluon radiation as a series of color-electric dipole transitions. In this way the NMEs are represented in an explicit form inspired by the classical multipole radiation theory, that leads to unpolarized or only weakly polarized mesons either because of the cancellation between the $^3P_1^{(8)}$ and $^3P_2^{(8)}$ contributions or as a result of two successive color-electric $E1$ dipole transitions in the chain $^3S_1^{(8)} \rightarrow {}^3P_J^{(8)} \rightarrow {}^3S_1^{(1)}$. This scenario was already successfully applied to describe the recent data on charmonia production and polarization [27,28]. Of course, it is important to investigate the bottomonia production within the same framework.

Springer

The data on $\Upsilon(nS)$ and $\chi_b(mP)$ mesons have been reported recently by the CMS [29,30], ATLAS [31] and LHCb [32,33] Collaborations at $\sqrt{s} = 7$, 8 and 13 TeV. As it was shown [34–38], these data can be explained within the NRQCD, both in polarization and yield. Our present study continues the line started in the previous paper [19] and here we consider the production and polarization of $\Upsilon(2S)$ mesons. To preserve the consistency with our studies [27,28], we apply the k_T-factorization QCD approach [39–42] to describe the perturbative production of the $b\bar{b}$ pair in the hard scattering subprocess. This approach is based on the Balitsky-Fadin-Kuraev-Lipatov (BFKL) [43–45] or Ciafaloni-Catani-Fiorani-Marchesini (CCFM) [46–49] evolution equations, which resum large logarithmic terms proportional to $\ln s \sim \ln 1/x$, important at high energies (or, equivalently, at low longitudinal momentum fraction x of proton carried by gluon). Resummation of the terms $\alpha_s^n \ln^n 1/x$, $\alpha_s^n \ln^n \mu^2/\Lambda_{\rm QCD}^2$ and $\alpha_s^n \ln^n 1/x \ln^n \mu^2/\Lambda_{\rm QCD}^2$ up to all orders in the perturbative expansion results in Transverse Momentum Dependent (TMD) gluon distributions, that generalize the factorization of hadronic amplitudes beyond the conventional (collinear) DGLAP-based approximation. For the different aspects of the k_T-factorization approach the reader may consult the reviews [50]. We determine the NMEs for $\Upsilon(2S)$ and $\chi_b(2P)$ mesons from the $\Upsilon(2S)$ transverse momentum distributions measured by the CMS [29,30] and ATLAS [31] Collaborations at $\sqrt{s} = 7$ and 13 TeV and from the relative production ratio $R_{\Upsilon(2S)}^{\chi_b(2P)}$ measured by the LHCb Collaboration at $\sqrt{s} = 7$ and 8 TeV [51]. In the calculations we take into account the feed-down contributions from $\chi_b(3P)$, $\chi_b(2P)$ and $\Upsilon(3S)$ decays. Then, we make predictions for polarization parameters λ_θ, λ_ϕ, $\lambda_{\theta\phi}$ (and frame-independent parameter $\tilde{\lambda}$), which determine the $\Upsilon(2S)$ spin density matrix and compare them to the currently available data [20,24].

The outline of our paper is the following. In Sect. 2 we briefly recall the basic steps of our calculations. In Sect. 3 we perform a numerical fit and extract the NMEs from the LHC data. Then we test the compatibility of the extracted NMEs with the available LHCb data on $\Upsilon(2S)$ transverse momentum distributions and Tevatron data on the $\Upsilon(2S)$ transverse momentum distributions and polarization. Our conclusions are collected in Sect. 4.

2 Theoretical framework

In the present paper we follow mostly the same steps as in our previous paper [19]. Our consideration is based on the off-shell gluon-gluon fusion subprocesses that represents the true leading order (LO) in QCD:

$$g^*(k_1) + g^*(k_2) \to \Upsilon\left[^3S_1^{(1)}\right](p) + g(k), \tag{1}$$

$$g^*(k_1) + g^*(k_2) \to \Upsilon\left[^1S_0^{(8)}, {}^3S_1^{(8)}, {}^3P_J^{(8)}\right](p), \tag{2}$$

$$g^*(k_1) + g^*(k_2) \to \chi_{bJ}(p)\left[^3P_J^{(1)}, {}^3S_1^{(8)}\right]$$
$$\to \Upsilon(p_1) + \gamma(p_2), \tag{3}$$

where we listed all intermediate color states, $J = 0, 1$ or 2 and the four-momenta of all particles are indicated in the parentheses. The respective cross sections for $2 \to 2$ and $2 \to 1$ subprocesses are:

$$\sigma = \int \frac{1}{8\pi (x_1 x_2 s) F} f_g\left(x_1, \boldsymbol{k}_{1T}^2, \mu^2\right) f_g\left(x_2, \boldsymbol{k}_{2T}^2, \mu^2\right)$$
$$\times \overline{|A(g^* + g^* \to \mathcal{Q} + g)|^2} d\boldsymbol{p}_T^2 d\boldsymbol{k}_{1T}^2 d\boldsymbol{k}_{2T}^2 dy dy_g$$
$$\times \frac{d\phi_1}{2\pi} \frac{d\phi_2}{2\pi}, \tag{4}$$

$$\sigma = \int \frac{2\pi}{x_1 x_2 s F} f_g\left(x_1, \boldsymbol{k}_{1T}^2, \mu^2\right) f_g$$
$$\times \left(x_2, \boldsymbol{k}_{2T}^2, \mu^2\right) \overline{|A(g^* + g^* \to \mathcal{Q})|^2} d\boldsymbol{k}_{1T}^2 d\boldsymbol{k}_{2T}^2 dy$$
$$\times \frac{d\phi_1}{2\pi} \frac{d\phi_2}{2\pi}, \tag{5}$$

where $\mathcal{Q}$ is the Υ and/or χ_b meson, ϕ_1 and ϕ_2 are the azimuthal angles of initial off-shell gluons having the longitudinal momentum fractions x_1 and x_2, $\boldsymbol{p}_T$ and y are the transverse momentum and rapidity of produced mesons, y_g is the rapidity of outgoing gluon and F is the off-shell flux factor [52]. The initial off-shell gluons have non-zero transverse momenta $\boldsymbol{k}_{1T}^2 \neq 0$, $\boldsymbol{k}_{2T}^2 \neq 0$ and an admixture of longitudinal component in the polarization vectors. So, the gluon spin density matrix is taken in the form $\sum \epsilon^\mu \epsilon^{*\nu} = \boldsymbol{k}_T^\mu \boldsymbol{k}_T^\nu / \boldsymbol{k}_T^2$,
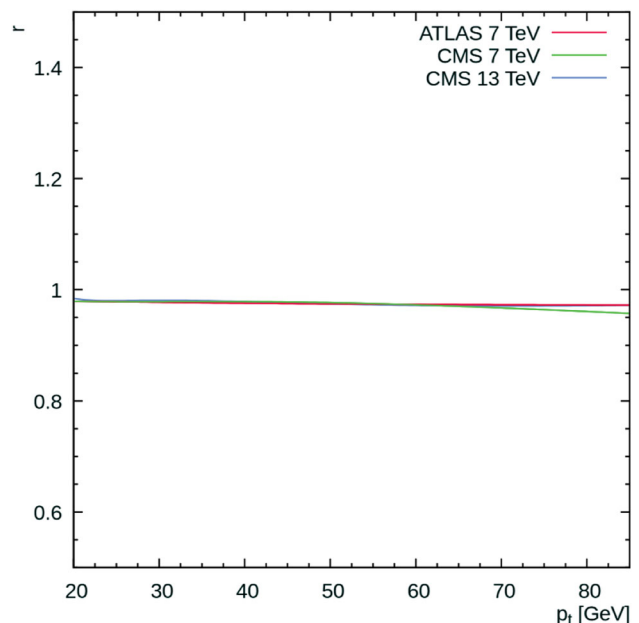

Fig. 1 The production ratio $r(p_t)$ calculated as a function of $\Upsilon(2S)$ transverse momentum p_T in the different kinematical regions

Table 1 The NMEs for $\Upsilon(3S)$ and $\chi_b(3P)$ mesons as determined from our fit at $p_T^{\text{cut}} = 10$ GeV. The NMEs obtained in the NLO NRQCD [37] are shown for comparison

	A0	JH'2013 set 1	KMR	PB'2018 set 2	NLO NRQCD [37]
$\langle \mathcal{O}^{\Upsilon(3S)}[^3S_1^{(1)}] \rangle/\text{GeV}^3$	3.22	3.22	3.22	3.22	3.54
$\langle \mathcal{O}^{\Upsilon(3S)}[^1S_0^{(8)}] \rangle/\text{GeV}^3$	0.0	0	0.0	0.0	0.0145 ± 0.0116
$\langle \mathcal{O}^{\Upsilon(3S)}[^3S_1^{(8)}] \rangle/\text{GeV}^3$	0.018 ± 0.001	0.007 ± 0.002	0.006 ± 0.001	0.018 ± 0.003	0.0132 ± 0.0020
$\langle \mathcal{O}^{\Upsilon(3S)}[^3P_0^{(8)}] \rangle/\text{GeV}^5$	0.0	0.09 ± 0.03	0.073 ± 0.006	0.73 ± 0.02	-0.0027 ± 0.0025
$\langle \mathcal{O}^{\chi_{b0}(3P)}[^3P_0^{(1)}] \rangle/\text{GeV}^5$	2.84	2.84	2.84	2.84	2.57
$\langle \mathcal{O}^{\chi_{b0}(3P)}[^3S_1^{(8)}] \rangle/\text{GeV}^3$	0.016 ± 0.003	0.009 ± 0.001	0.005 ± 0.001	0.048 ± 0.005	0.0069 ± 0.0014

Table 2 The NMEs for $\Upsilon(2S)$ and $\chi_b(2P)$ mesons as determined from our fit at $p_T^{\text{cut}} = 10$ GeV. The NMEs obtained in the NLO NRQCD [37] are shown for comparison

	A0	JH'2013 set 1	KMR	PB'2018 set 2	NLO NRQCD [37]
$\langle \mathcal{O}^{\Upsilon(2S)}[^3S_1^{(1)}] \rangle/\text{GeV}^3$	4.15	4.15	4.15	4.15	4.63
$\langle \mathcal{O}^{\Upsilon(2S)}[^1S_0^{(8)}] \rangle/\text{GeV}^3$	0.0	0.0	0.0	0.0	0.0062 ± 0.0198
$\langle \mathcal{O}^{\Upsilon(2S)}[^3S_1^{(8)}] \rangle/\text{GeV}^3$	0.024 ± 0.004	0.007 ± 0.007	0.006 ± 0.0007	0.0	0.0222 ± 0.0024
$\langle \mathcal{O}^{\Upsilon(2S)}[^3P_0^{(8)}] \rangle/\text{GeV}^5$	0.014 ± 0.009	0.19 ± 0.05	0.14 ± 0.02	1.15 ± 0.07	-0.0013 ± 0.0043
$\langle \mathcal{O}^{\chi_{b0}(2P)}[^3P_0^{(1)}] \rangle/\text{GeV}^5$	2.61	2.61	2.61	2.61	2.37
$\langle \mathcal{O}^{\chi_{b0}(2P)}[^3S_1^{(8)}] \rangle/\text{GeV}^3$	0.0096 ± 0.0005	0.0061 ± 0.0004	0.003 ± 0.0003	0.045 ± 0.009	0.0109 ± 0.0014

Table 3 The dependence of the $\chi^2/d.o.f.$ achieved in the fit procedure on the choice of p_T^{cut} at only $\sqrt{s} = 7$ TeV and at 7 and 13 TeV combined

7 TeV	$p_T^{\text{cut}} = 10$ GeV	$p_T^{\text{cut}} = 12$ GeV	$p_T^{\text{cut}} = 15$ GeV	$p_T^{\text{cut}} = 17$ GeV
A0	1.34	1.29	1.25	1.31
JH'2013 set 1	2.84	2.32	1.94	1.94
KMR	1.62	1.63	1.67	1.76
PB'2018 set 2	1.59	1.63	1.71	1.81
7 + 13 TeV	$p_T^{\text{cut}} = 10$ GeV	$p_T^{\text{cut}} = 12$ GeV	$p_T^{\text{cut}} = 15$ GeV	$p_T^{\text{cut}} = 17$ GeV
A0	2.72	2.73	2.77	2.86
JH'2013 set 1	6.28	6.08	5.99	6.14
KMR	3.25	3.32	3.4	3.52
PB'2018 set 2	3.66	3.77	3.89	4.03

where $\boldsymbol{k}_T$ is the component of the gluon momentum perpendicular to the beam axis [39–42]. In the collinear limit $\boldsymbol{k}_T \to 0$ this expression converges to the ordinary one $\sum \epsilon^\mu \epsilon^{*\nu} = -1/2g^{\mu\nu}$. In all other respects, we follow the standard QCD Feynman rules. As usual, the hard production amplitudes contain spin and color projection operators [53–56] that guarantee the proper quantum numbers of the state under consideration (see, for example, [19,27,28] for more details).

The formation of $b\bar{b}$ bound states need additional explanation. We employ the mechanism[1] proposed in [26] and

used previously [19,27,28]. A soft gluon with a small energy $E \sim \Lambda_{\text{QCD}}$ is emitted after the hard interaction is over, bringing away the unwanted color and changing other quantum numbers of the produced CO system. In our calculations such soft gluon emission is described by a classical multipole expansion, in which the electric dipole ($E1$) transition dominates [57,58]. Only a single $E1$ transition is needed to transform a P-wave state into an S-wave state and the structure of the respective $^3P_J^{(8)} \to {}^3S_1^{(1)} + g$ amplitudes is given by [57,58]:

---

[1] The mechanism [26] is not connected to the choice of factorization scheme (k_T or collinear), but represents a completely independent issue.

$$A\left({}^3P_0^{(8)} \to \Upsilon + g\right) \sim k_\mu^{(g)} p^{(CO)\mu} \epsilon_\nu^{(\Upsilon)} \epsilon^{(g)\nu}, \qquad (6)$$

$$A\left({}^3P_1^{(8)} \to \Upsilon + g\right) \sim e^{\mu\nu\alpha\beta} k_\mu^{(g)} \epsilon_\nu^{(CO)} \epsilon_\alpha^{(\Upsilon)} \epsilon_\beta^{(g)}, \qquad (7)$$
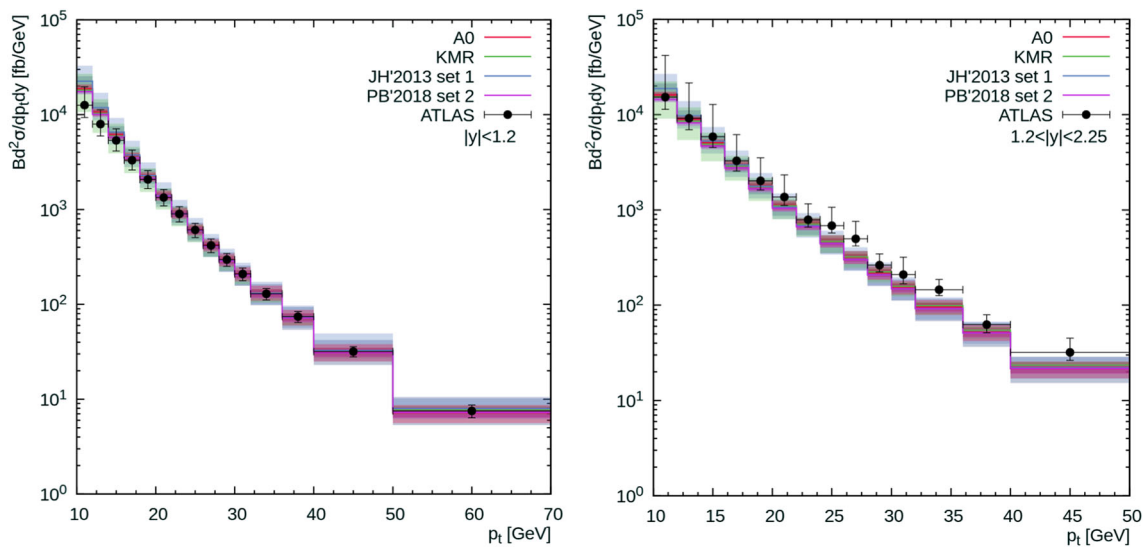
Fig. 2 Transverse momentum distribution of inclusive $\Upsilon(2S)$ production calculated at $\sqrt{s} = 7$ TeV in the different rapidity regions. The red, green, blue and violet histograms correspond to the predictions obtained with A0, KMR, JH'2013 set 1 and PB gluon densities. Shaded bands represent the total uncertainties of our calculations, as it is described in text. The experimental data are from ATLAS [31]

$$A \left({}^3P_2^{(8)} \rightarrow \Upsilon + g \right) \sim p_\mu^{(CO)} \epsilon_{\alpha\beta}^{(CO)} \epsilon_\alpha^{(\Upsilon)}$$
$$\times \left[k_\mu^{(g)} \epsilon_\beta^{(g)} - k_\beta^{(g)} \epsilon_\mu^{(g)} \right], \qquad (8)$$

where $p_\mu^{(CO)}$, $k_\mu^{(g)}$, $\epsilon_\mu^{(\Upsilon)}$, $\epsilon_\mu^{(g)}$, $\epsilon_\mu^{(CO)}$ and $\epsilon_\mu^{(CO)}$ are the momenta and polarization vectors of corresponding particles and $e^{\mu\nu\alpha\beta}$ is the fully antisymmetric Levi-Civita tensor. The transformation of color-octet S-wave state into the color-singlet S-wave state is treated as two successive $E1$ transitions ${}^3S_1^{(8)} \rightarrow {}^3P_J^{(8)} + g$, ${}^3P_J^{(8)} \rightarrow {}^3S_1^{(1)} + g$ proceeding via either of three intermediate ${}^3P_J^{(8)}$ states with $J = 0, 1, 2$. For each of these transitions we apply the same expressions (6)–(8). The amplitudes (6)–(8) lead to the fact that the final state bottomonia come unpolarized [26], either because of the cancellation between the ${}^3P_1^{(8)}$ and ${}^3P_2^{(8)}$ contributions or as a result of two successive $E1$ transitions. This property remains true irrespectively of the numerical values of NMEs and only follows from the spin algebra. The expressions (6)–(8) can be applied for both gluons and photons (up to an overall color factor) and can be used to calculate the polarization variables in radiative decays in feed-down processes.

As we did in our previous paper [19], we have tested several sets of TMD gluon densities in a proton. Two of them (A0 [59] and JH'2013 set 1 [60]) were obtained from CCFM equation where all input parameters were fitted to the proton structure function $F_2(x, Q^2)$. Next, we have applied a parametrization obtained within the Kimber-Martin-Ryskin (KMR) prescription [61–63], which provides a method to construct the TMD quark and gluon densities from conventional (collinear) distributions. For the input, we have used

the recent LO NNPDF3.1 set [64]. Besides that, we have tested the TMD gluon distribution obtained in the recently proposed Parton Branching (PB) approach [65,66]. This approach provides an iterative solution of the DGLAP evolution equations for both the collinear and TMD parton distributions by making use of the concept of resolvable and non-resolvable branchings. To be precise, we have applied PB-NLO-HERAI+II'2018 set 2 [67].

The parton level calculations were performed using the Monte-Carlo event generator PEGASUS [68].

3 Numerical results

In the present paper we set the masses $m_{\Upsilon(2S)} = 10.02326$ GeV, $m_{\chi_{b1}(3P)} = 10.512$ GeV, $m_{\chi_{b2}(3P)} = 10.522$ GeV, $m_{\chi_{b0}(2P)} = 10.232$ GeV, $m_{\chi_{b1}(2P)} = 10.255$ GeV, $m_{\chi_{b2}(2P)} = 10.268$ GeV [69] and adopt the usual non-relativistic approximation $m_b = m_{\mathcal{Q}}/2$ for the beauty quark mass, where $m_{\mathcal{Q}}$ is the mass of bottomonium $\mathcal{Q}$. We set the branching ratios $B(\Upsilon(2S) \rightarrow \mu^+\mu^-) = 0.0193$, $B(\Upsilon(3S) \rightarrow \Upsilon(2S) + X) = 0.1060$, $B(\chi_{b0}(2P) \rightarrow \Upsilon(2S) + \gamma) = 0.0138$, $B(\chi_{b1}(2P) \rightarrow \Upsilon(2S) + \gamma) = 0.1810$, $B(\chi_{b2}(2P) \rightarrow \Upsilon(2S) + \gamma) = 0.0890$ [69], $B(\chi_{b1}(3P) \rightarrow \Upsilon(2S) + \gamma) = 0.0368$ and $B(\chi_{b2}(3P) \rightarrow \Upsilon(2S) + \gamma) = 0.0191$ [38]. Note that there is no experimental data for branching ratios of $\chi_b(3P)$, so the values above are the results of assumption [38] that the total decay widths of $\chi_b(mP)$ are approximately independent on m. We use the one-loop formula for the QCD coupling α_s with $n_f = 4(5)$ quark flavours at $\Lambda_{QCD} = 250(167)$ MeV for
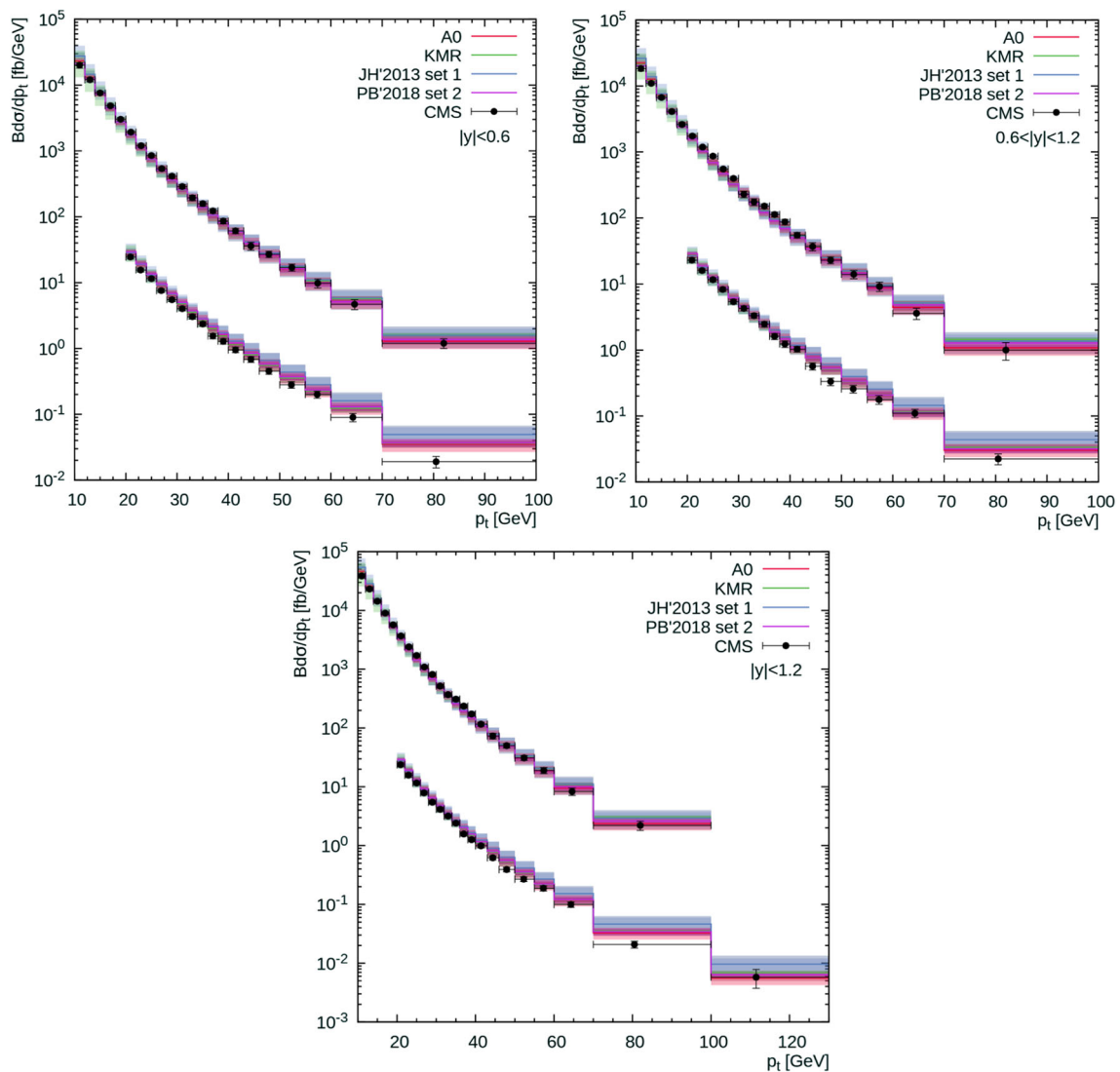
Fig. 3 Transverse momentum distribution of inclusive $\Upsilon(2S)$ production calculated at $\sqrt{s} = 7$ TeV (upper histograms) and $\sqrt{s} = 13$ TeV (lower histograms, divided by 100) in the different rapidity regions. Notation of all histograms is the same as in Fig. 2. The experimental data are from CMS [29,30]

A0 (KMR) gluon density and two-loop expression for α_s with $n_f = 4$ and $\Lambda_{QCD} = 200$ MeV for JH'2013 set 1 one. In the case of the PB gluon, we apply the two-loop QCD coupling with $n_f = 4$ and $\Lambda_{QCD} = 118$ MeV. These parameters were obtained from best description of the structure function $F_2(x, Q^2)$ [59–63,65,66]. We set color-singlet NMEs $\langle\mathcal{O}^{\Upsilon(2S)}[^3S_1^{(1)}]\rangle = 4.15$ GeV^3 and $\langle\mathcal{O}^{\chi_{b0}(2P)}[^3P_0^{(1)}]\rangle = 2.61$ GeV^5 as obtained from the potential model calculations [70]. All the NMEs for $\Upsilon(3S)$ and $\chi_b(3P)$ mesons were derived in [19].

3.1 Fit of color octet NMEs

We performed a global fit to the $\Upsilon(2S)$ production data at the LHC and determined the corresponding NMEs for both $\Upsilon(2S)$ and $\chi_b(2P)$ mesons. We have included in the fitting procedure the $\Upsilon(2S)$ transverse momentum distributions measured by the CMS [29,30] and ATLAS [31] Collaborations at $\sqrt{s} = 7$ and 13 TeV. To determine NMEs for $\chi_b(2P)$ mesons, we also included into the fit the recent LHCb data [51] on the radiative $\chi_b(2P) \rightarrow \Upsilon(2S) + \gamma$ decays collected at $\sqrt{s} = 7$ and 8 TeV. We have excluded from our fit low p_T region and consider only the data at $p_T > p_T^{cut} = 10$ GeV, where the NRQCD formalism is believed to be most reliable.

We would like to mention here a few important points. First of all, we found that the p_T shape of the direct $\Upsilon[^3S_1^{(8)}]$ and feed-down $\chi_b[^3S_1^{(8)}]$ contributions to $\Upsilon(2S)$ production is almost the same in all kinematical regions probed at the LHC. Thus, the ratio
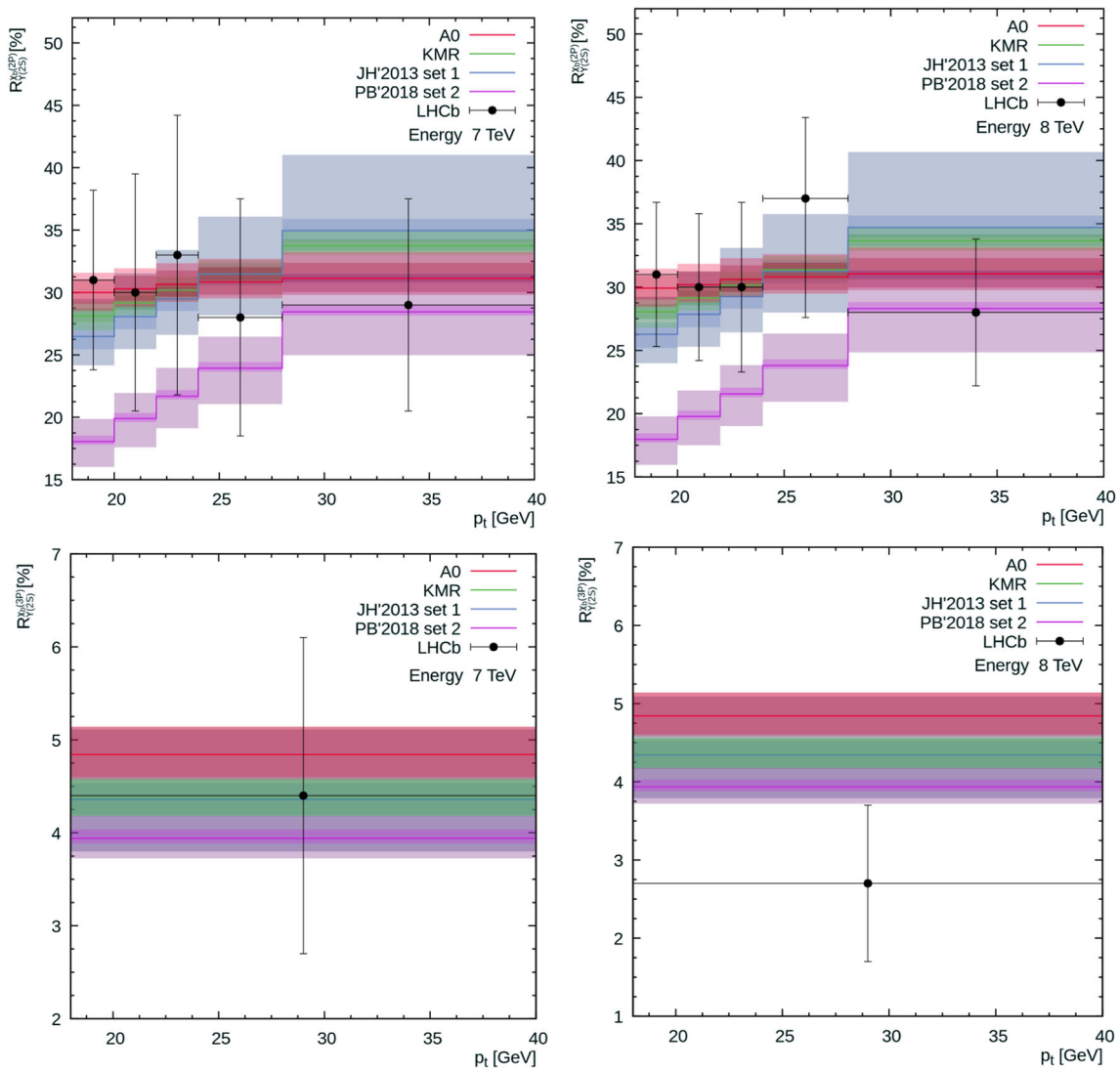
Fig. 4 The ratio $R_{\Upsilon(2S)}^{\chi_b(mP)}$ calculated as function of $\Upsilon(2S)$ transverse momentum. Notation of all histograms is the same as in Fig. 2. The experimental data are from LHCb [51]

$$r = \frac{\sum_{J=0}^{2}(2J+1)\,B(\chi_{bJ}(2P) \to \Upsilon(2S)+\gamma)d\sigma\left[\chi_{bJ}(2P),{}^3S_1^{(8)}\right]/dp_T}{d\sigma\left[\Upsilon(2S),{}^3S_1^{(8)}\right]/dp_T}$$

(9)

can be well approximated by a constant for a wide $\Upsilon(2S)$ transverse momentum p_T and rapidity y ranges at different energies, as seen in Fig. 1. We estimate the mean-square average $r = 0.98 \pm 0.005$, which is practically independent on the TMD gluon density in a proton. So that, we construct the linear combination

$$M_r = \left\langle \mathcal{O}^{\Upsilon(2S)}\left[{}^3S_1^{(8)}\right]\right\rangle + r \left\langle \mathcal{O}^{\chi_{b0}(2P)}\left[{}^3S_1^{(8)}\right]\right\rangle,$$

(10)

which can be only extracted from the measured $\Upsilon(2S)$ transverse momentum distributions. Then we use recent LHCb data [51] on the ratio of $\Upsilon(2S)$ mesons originating from the

$\chi_b(2P)$ radiative decays measured at $\sqrt{s} = 7$ and 8 TeV:

$$R_{\Upsilon(2S)}^{\chi_b(2P)} = \sum_{J=0}^{2} \frac{\sigma(pp \to \chi_{bJ}(2P)+X)}{\sigma(pp \to \Upsilon(2S)+X)}$$
$$\times B(\chi_{bJ} \to \Upsilon(2S)+\gamma).$$

(11)

From the known M_r and $R_{\Upsilon(2S)}^{\chi_b(2P)}$ values one can separately determine the $\langle \mathcal{O}^{\Upsilon(2S)}[{}^3S_1^{(8)}]\rangle$ and $\langle \mathcal{O}^{\chi_{b0}(2P)}[{}^3S_1^{(8)}]\rangle$ and, therefore, reconstruct full map of color octet NMEs for both $\Upsilon(2S)$ and $\chi_b(2P)$ mesons.

The fitting procedure was separately done in each of the rapidity subdivisions (using the fitting algorithm as implemented in the commonly used GNUPLOT package [71]) under the requirement that all the NMEs be strictly positive. Then, the mean-square average of the fitted values was taken. The corresponding uncertainties are estimated in the conventional
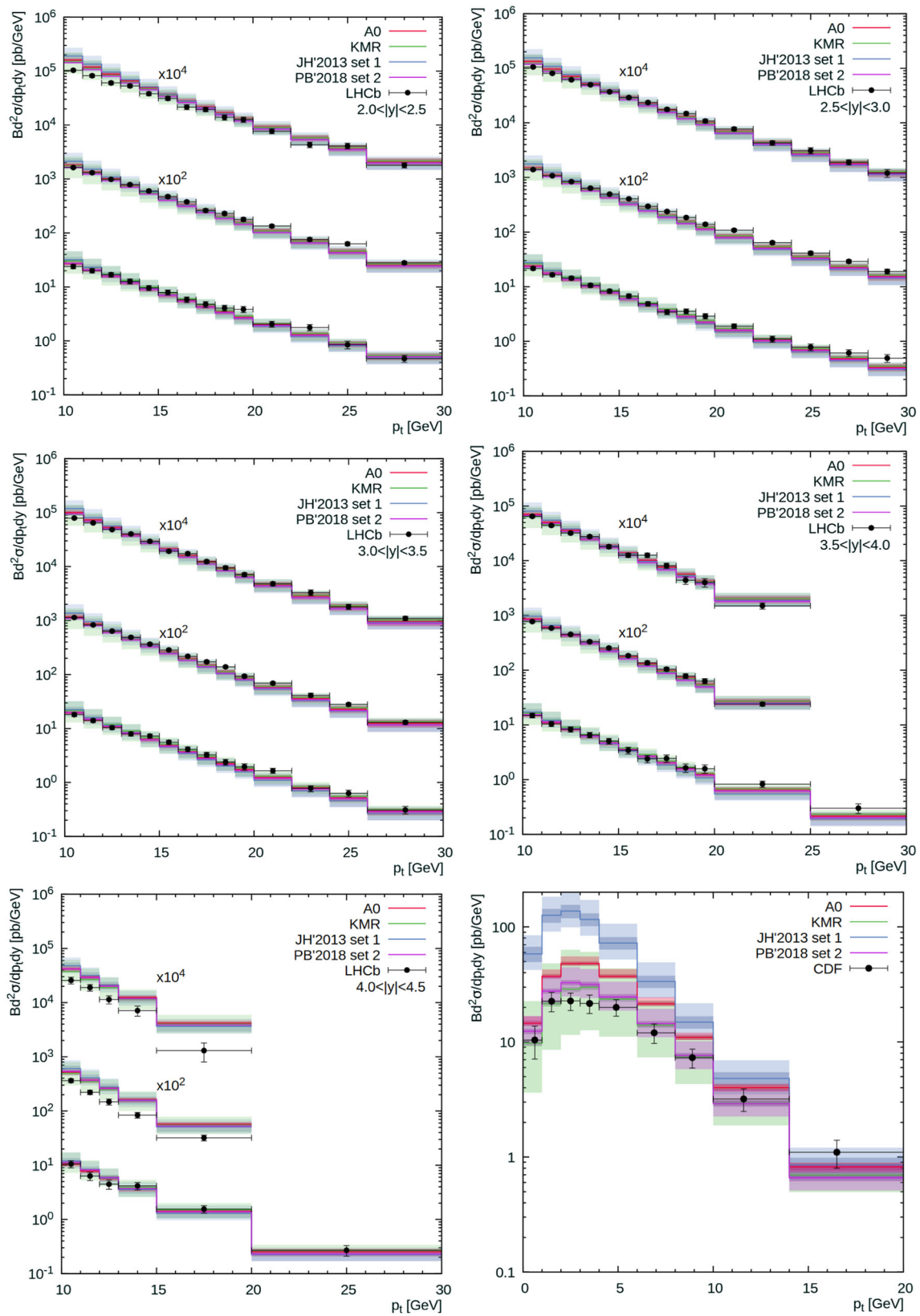
Fig. 5 Transverse momentum distribution of inclusive $\Upsilon(2S)$ production calculated at $\sqrt{s} = 1.8, 7, 8$ and 13 TeV in the different rapidity regions. Notation of all histograms is the same as in Fig. 2. The experimental data are from CDF [75] and LHCb [32,33]
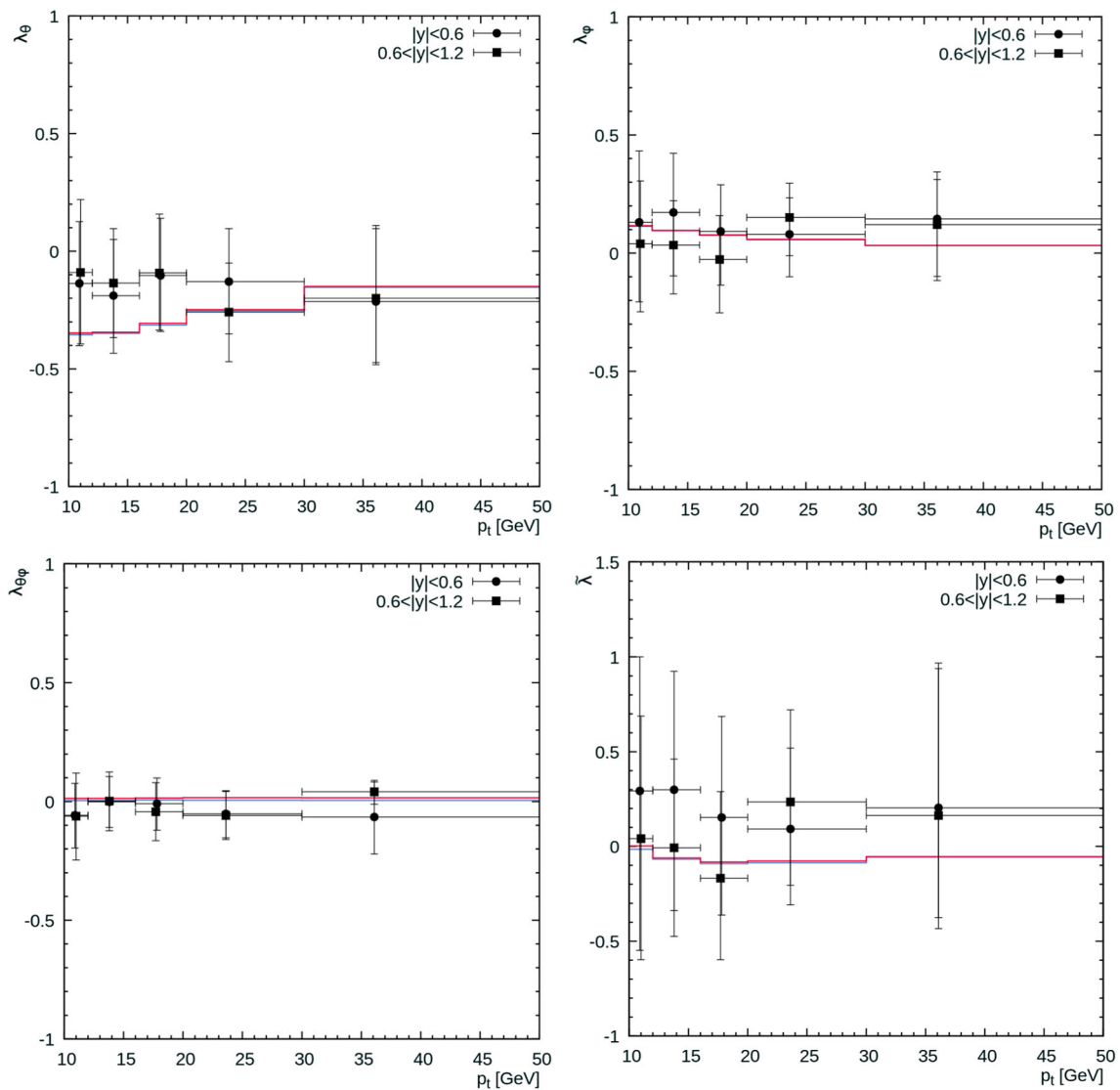
Fig. 6 The polarization parameters λ_θ, λ_ϕ, $\lambda_{\theta\phi}$ and $\tilde{\lambda}$ of $\Upsilon(2S)$ mesons calculated in the CS frame as function of its transverse momentum at $\sqrt{s} = 7$ TeV. The A0 gluon density is used. The blue and red histograms correspond to the predictions obtained at $|y| < 0.6$ and $0.6 < |y| < 1.2$, respectively. The experimental data are from CMS [20]

way using Student's t-distribution at the confidence level $P = 80\%$. The results of our fits are collected in Tables 1 and 2. For comparison, we also presented there the NMEs obtained in the conventional NLO NRQCD by other authors [37]. We note that the NMEs for $\Upsilon(3S)$ and $\Upsilon(2S)$ mesons extracted with the PB gluon density differ from the ones derived using the CCFM-evolved gluon distributions, that reflect the essential DGLAP dynamics and absence of the small-x enhanced terms in the PB scenario.[2] The corresponding $\chi^2/d.o.f.$ are listed in Table 3, where we addi-

tionally show their dependence on the minimal $\Upsilon(2S)$ transverse momenta involved into the fit p_T^{cut}. As one can see, the $\chi^2/d.o.f.$ tends to decrease when p_T^{cut} grows up and best fit of the LHC data is achieved with A0 gluon, although other gluon densities also return reliable $\chi^2/d.o.f.$ values. We note that including into the fit the latest CMS data [30] taken at $\sqrt{s} = 13$ TeV leads to 2–3 times higher values of $\chi^2/d.o.f.$ We have checked that this is true for both the k_T-factorization and collinear approaches[3] and, therefore, it could be a sign of some inconsistency between these CMS data and all other measurements.

---

[2] Relation between the CCFM and PB scenarios have been discussed recently [72] and relation between the PB and KMR schemes have been also studied [73,74].

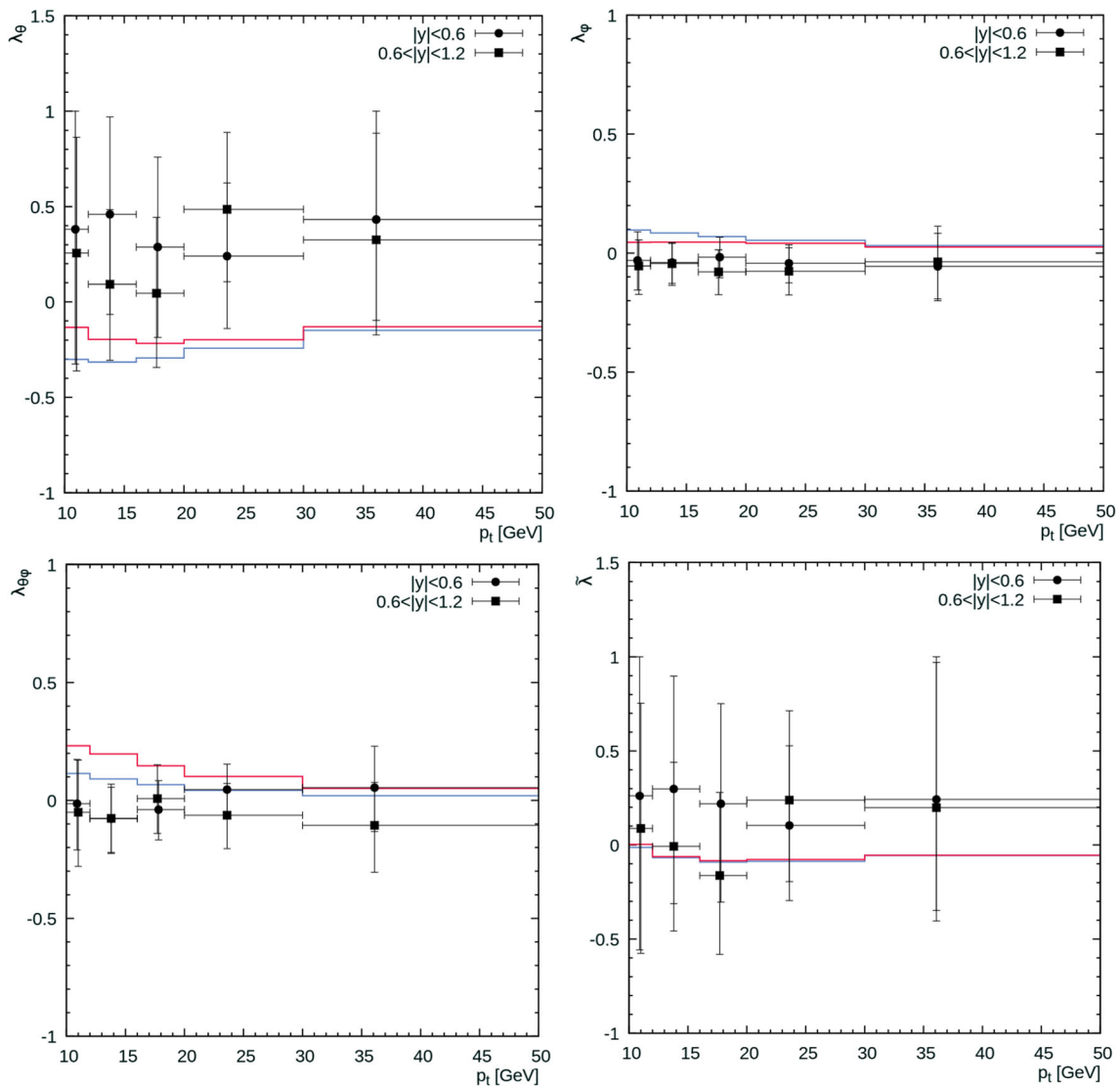[3] We have used the on-shell production amplitudes for color-octet $2 \to 2$ subprocesses from [18].

Fig. 7 The polarization parameters λ_θ, λ_ϕ, $\lambda_{\theta\phi}$ and $\tilde{\lambda}$ of $\Upsilon(2S)$ mesons calculated in the helicity frame as function of its transverse momentum at $\sqrt{s} = 7$ TeV. Notation of all histograms is the same as in Fig. 6. The experimental data are from CMS [20]

All the data used in the fits are compared with our predictions in Figs. 2, 3 and 4. The shaded areas represent the theoretical uncertainties of our calculations, which include the scale uncertainties, uncertainties coming from the NME fitting procedure and uncertainties connected with the choice of the intermediate color-octet mass, added in quadrature. To estimate the scale uncertainties the standard variations $\mu_R \rightarrow 2\mu_R$ or $\mu_R \rightarrow \mu_R/2$ were introduced with replacing the A0 and JH'2013 set 1 gluon densities by A0+ and JH'2013 set 1+, or by A0− and JH'2013 set 1− ones. This was done to preserve the intrinsic correspondence between the TMD gluon set and the scale used in the CCFM evolution [59,60]. To estimate the uncertainties connected with the intermediate color-octet mass we have varied amount of energy E emitted in the course of transition of unbound color

octet $b\bar{b}$ pair into the observed bottomonium by a factor of 2 around its default value $E = \Lambda_{\text{QCD}}$. One can see that we have achieved a reasonably good description of the CMS [29,30] and ATLAS [31] data in a whole p_T range within the experimental and theoretical uncertainties for the $\Upsilon(2S)$ transverse momentum distributions. The ratios $R_{\Upsilon(2S)}^{\chi_b(2P)}$ and $R_{\Upsilon(2S)}^{\chi_b(3P)}$ measured by the LHCb Collaboration [51] at $\sqrt{s} = 7$ and 8 TeV are also reproduced well, see Fig. 5.

Finally, we have checked our results with the data, not included into the fit procedure: namely, rather old CDF data [75] taken at the $\sqrt{s} = 1.8$ TeV and LHCb data [32,33] taken in the forward rapidity region $2 < y < 4.5$ at $\sqrt{s} = 7$, 8 and 13 TeV (see Fig. 6). As one can see, we acceptably describe all the data above. Moreover, we find that the KMR and PB
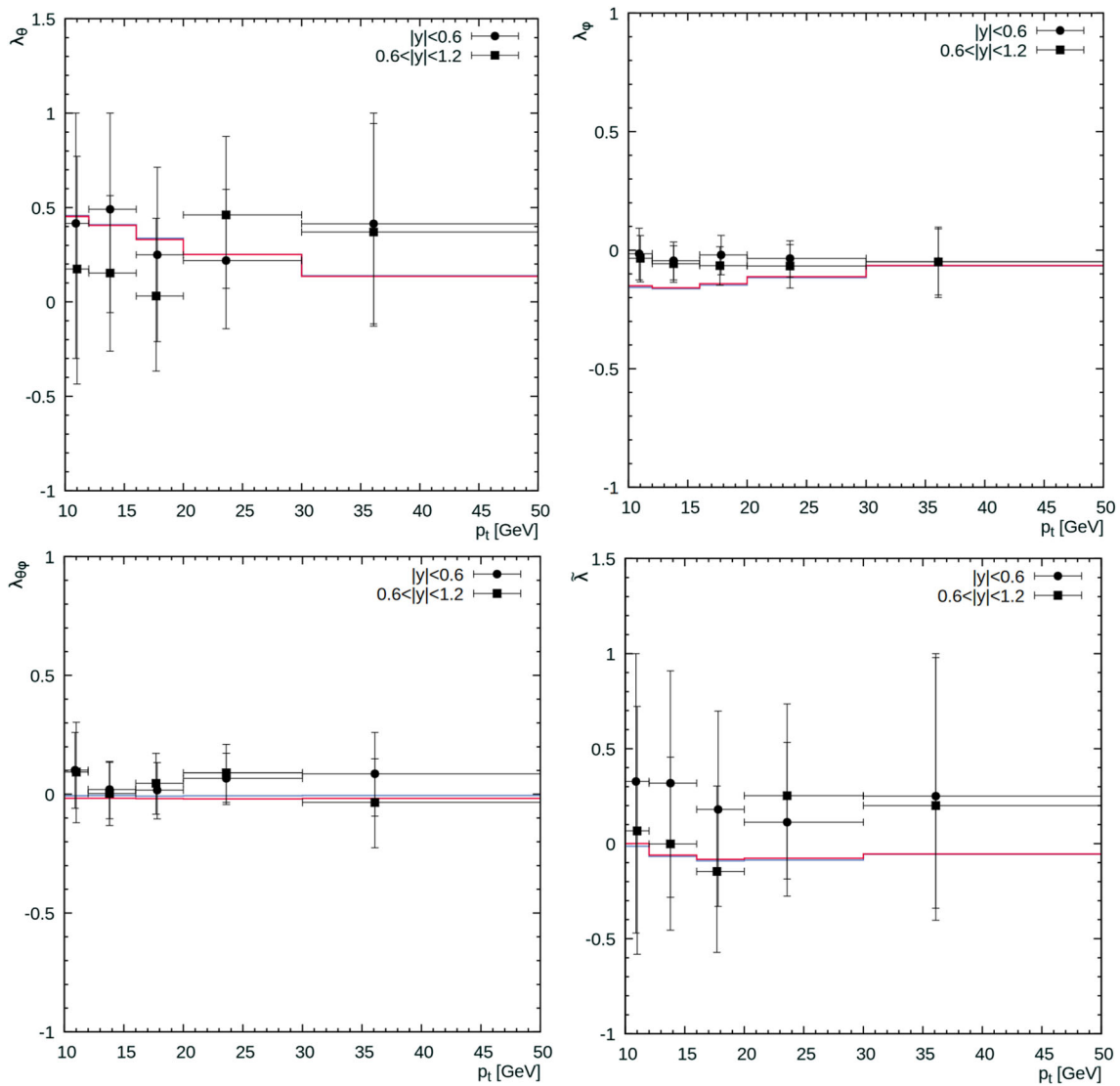
Fig. 8 The polarization parameters λ_θ, λ_ϕ, $\lambda_{\theta\phi}$ and $\tilde{\lambda}$ of $\Upsilon(2S)$ mesons calculated in the perpendicular helicity frame as function of its transverse momentum at $\sqrt{s} = 7$ TeV. Notation of all histograms is the same as in Fig. 6. The experimental data are from CMS [20]

densities are only TMD gluon distributions which are able to reproduce the measurements in the low p_T region.

3.2 $\Upsilon(2S)$ polarization

The polarization of any vector meson can be described with three parameters λ_θ, λ_ϕ and $\lambda_{\theta\phi}$, which determine the spin density matrix of a meson decaying into a lepton pair and can be measured experimentally. The double differential angular distribution of the decay leptons can be written as [76]:

$$\frac{d\sigma}{d\cos\theta^* d\phi^*} \sim \frac{1}{3+\lambda_\theta}(1 + \lambda_\theta \cos^2\theta^* + \lambda_\phi \sin^2\theta^* \cos 2\phi^* + \lambda_{\theta\phi} \sin 2\theta^* \cos\phi^*), \quad (12)$$

where θ^* and ϕ^* are the polar and azimuthal angles of the decay lepton measured in the meson rest frame. The case of $(\lambda_\theta, \lambda_\phi, \lambda_{\theta\phi}) = (0, 0, 0)$ corresponds to unpolarized state, while $(\lambda_\theta, \lambda_\phi, \lambda_{\theta\phi}) = (1, 0, 0)$ and $(\lambda_\theta, \lambda_\phi, \lambda_{\theta\phi}) = (-1, 0, 0)$ refer to fully transverse and fully longitudinal polarizations.

The CMS Collaboration has measured all of these polarization parameters for $\Upsilon(2S)$ mesons as functions of their transverse momentum in three complementary frames: the Collins-Soper, helicity and perpendicular helicity ones at $\sqrt{s} = 7$ TeV [20]. The frame-independent parameter $\tilde{\lambda} = (\lambda_\theta + 3\lambda_\phi)/(1 - \lambda_\phi)$ has been additionally studied. The CDF Collaboration has measured λ_θ and $\tilde{\lambda}$ parameters in the helicity frame at $\sqrt{s} = 1.96$ TeV [24]. As it was done previously [19], to estimate λ_θ, λ_ϕ, $\lambda_{\theta\phi}$ and $\tilde{\lambda}$ we generally follow the
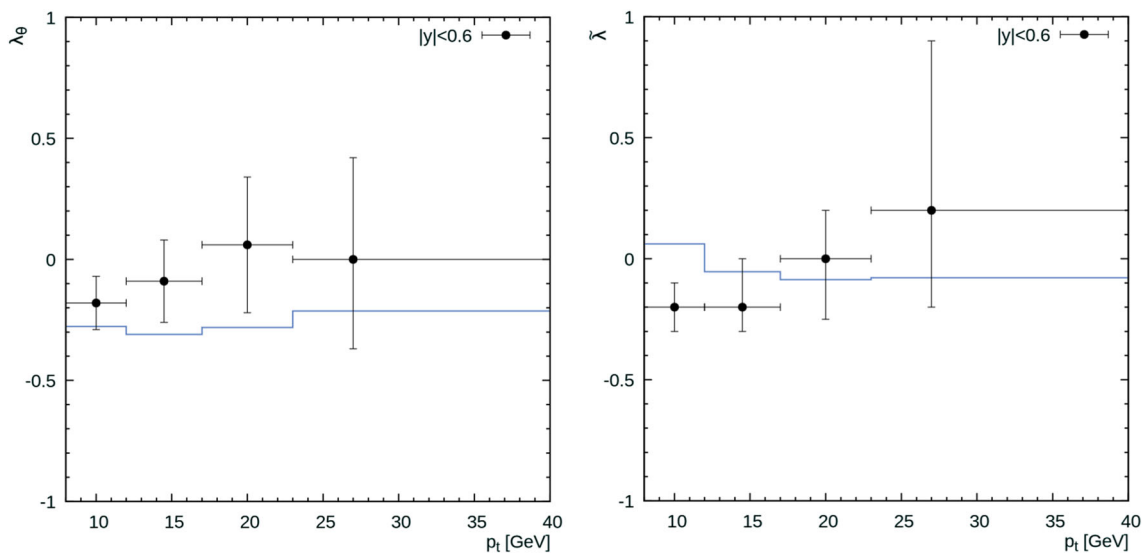
Fig. 9 The polarization parameters λ_θ and $\tilde{\lambda}$ of $\Upsilon(2S)$ mesons calculated in the helicity frame as function of its transverse momentum at $\sqrt{s} = 1.96$ TeV. Notation of all histograms is the same as in Fig. 6. The experimental data are from CDF [24]

experimental procedure. We collect the simulated events in the kinematical region defined by the experimental setup, generate the decay lepton angular distributions according to the production and decay matrix elements and then apply a three-parametric fit based on (12).

Our predictions are shown in Figs. 6, 7, 8 and 9. The calculations were done using the A0 gluon density which provides a best description of the measured $\Upsilon(2S)$ transverse momenta distributions. As one can see, we find only weak or zero polarization in the all kinematic regions, that agrees with the CMS and CDF measurements. The similar results we have obtained earlier for charmonia (J/ψ, ψ') and $\Upsilon(3S)$ polarization [19,27,28]. Thus, we conclude that the approach [26], which is a corner stone of our consideration, results in a self-consistent and simultaneous description of the entire charmonia family, $\Upsilon(2S)$ and $\Upsilon(3S)$ production data and therefore can provide an easy and natural solution to the long-standing quarkonia production and polarization puzzle.

4 Conclusion

We have considered the $\Upsilon(2S)$ production at the Tevatron and LHC in the framework of k_T-factorization approach. Our consideration was based on the off-shell production amplitudes for hard partonic subprocesses (including both color-singlet and color-octet contributions), NRQCD formalism for the formation of bound states and TMD gluon densities in a proton. The latter were derived from the CCFM evolution equation, KMR scheme and recently proposed PB approach. Treating the nonperturbative color octet transitions in terms of multipole radiation theory and taking into account feed-

down contributions from the radiative $\chi_b(3P)$ and $\chi_b(2P)$ decays and contribution from $\Upsilon(3S)$ decays, we extracted long-distance non-perturbative NRQCD matrix elements for $\Upsilon(2S)$ and $\chi_b(2P)$ mesons from a fit to $\Upsilon(2S)$ transverse momentum distributions measured by the CMS and ATLAS Collaborations at $\sqrt{s} = 7$ and 13 TeV and from the relative production rates $R^{\chi_b(2P)}_{\Upsilon(2S)}$ measured by the LHCb Collaboration at $\sqrt{s} = 7$ and 8 TeV. Then we estimated polarization parameters λ_θ, λ_ϕ, $\lambda_{\theta\phi}$ and frame-independent parameter $\tilde{\lambda}$ which determine the spin density matrix of $\Upsilon(2S)$ mesons. We show that treating the soft gluon emission as a series of explicit color-electric dipole transitions within the NRQCD leads to unpolarized $\Upsilon(2S)$ production at moderate and large transverse momenta, that is in agreement with the LHC data.

References

1. M. Krämer, Prog. Part. Nucl. Phys. **47**, 14 (2001)
2. J.P. Lansberg, Int. J. Mod. Phys. A **21**, 3857 (2006)
3. N. Brambilla et al., Eur. Phys. J. C **71**, 1534 (2011)
4. B. Gong, X.Q. Li, J.-X. Wang, Phys. Lett. B **673**, 197 (2009)
5. Y.-Q. Ma, K. Wang, K.-T. Chao, Phys. Rev. Lett. **106**, 042002 (2011)
6. M. Butenschön, B.A. Kniehl, Phys. Rev. Lett. **108**, 172002 (2012)
7. K.-T. Chao, Y.-Q. Ma, H.-S. Shao, K. Wang, Y.-J. Zhang, Phys. Rev. Lett. **108**, 242004 (2012)
8. B. Gong, L.-P. Wan, J.-X. Wang, H.-F. Zhang, Phys. Rev. Lett. **110**, 042002 (2013)
9. Y.-Q. Ma, K. Wang, K.-T. Chao, H.-F. Zhang, Phys. Rev. D **83**, 111503 (2011)
10. A.K. Likhoded, A.V. Luchinsky, S.V. Poslavsky, Phys. Rev. D **90**, 074021 (2014)
11. A.K. Likhoded, A.V. Luchinsky, S.V. Poslavsky, Mod. Phys. Lett. A **30**, 1550032 (2015)
12. H.-F. Zhang, L. Yu, S.-X. Zhang, L. Jia, Phys. Rev. D **93**, 054033 (2016)
13. H. Han, Y.-Q. Ma, C. Meng, H.-S. Shao, K.-T. Chao, Phys. Rev. Lett. **114**, 092005 (2015)
14. H.-F. Zhang, Z. Sun, W.-L. Sang, R. Li, Phys. Rev. Lett. **114**, 092006 (2015)
15. M. Butenschön, Z.G. He, B.A. Kniehl, Phys. Rev. Lett. **114**, 092004 (2015)
16. S.S. Biswal, K. Sridhar, J. Phys. G Nucl. Part. Phys. **39**, 015008 (2012)
17. G. Bodwin, E. Braaten, G. Lepage, Phys. Rev. D **51**, 1125 (1995)
18. P. Cho, A.K. Leibovich, Phys. Rev. D **53**, 150 (1996) **[Phys. Rev. D 53, 6203 (1996)]**
19. N.A. Abdulov, A.V. Lipatov, Eur. Phys. J. C **79**, 830 (2019)
20. CMS Collaboration, Phys. Rev. Lett. **110**, 081802 (2013)
21. CMS Collaboration, Phys. Lett. B **727**, 381 (2013)
22. LHCb Collaboration, Eur. Phys. J. C **74**, 2872 (2014)
23. CDF Collaboration, Phys. Rev. Lett. **99**, 132001 (2007)
24. CDF Collaboration, Phys. Rev. Lett. **108**, 151802 (2012)
25. P. Faccioli, V. Knuenz, C. Lourenco, J. Seixas, H.K. Woehri, Phys. Lett. B **736**, 98 (2014)
26. S.P. Baranov, Phys. Rev. D **93**, 054037 (2016)
27. S.P. Baranov, A.V. Lipatov, Eur. Phys. J. C **79**, 621 (2019)
28. S.P. Baranov, A.V. Lipatov, Phys. Rev. D **100**, 114021 (2019)
29. CMS Collaboration, Phys. Lett. B **749**, 14 (2015)
30. CMS Collaboration, Phys. Lett. B **780**, 251 (2018)
31. ATLAS Collaboration, Phys. Rev. D **87**, 052004 (2013)
32. LHCb Collaboration, JHEP **1511**, 103 (2015)
33. LHCb Collaboration, JHEP **1807**, 134 (2018)
34. B. Gong, J.-X. Wang, H.-F. Zhang, Phys. Rev. D **83**, 114021 (2011)
35. K. Wang, Y.-Q. Ma, K.-T. Chao, Phys. Rev. D **85**, 114003 (2012)
36. B. Gong, L.-P. Wan, J.-X. Wang, H.-F. Zhang, Phys. Rev. Lett. **112**, 032001 (2014)
37. Y. Feng, B. Gong, L.-P. Wan, J.-X. Wang, H.-F. Zhang, Chin. Phys. C **39**, 123102 (2015)
38. H. Han, Y.-Q. Ma, C. Meng, H.-S. Shao, Y.-J. Zhang, K.-T. Chao, Phys. Rev. D **94**, 014028 (2016)
39. L.V. Gribov, E.M. Levin, M.G. Ryskin, Phys. Rep. **100**, 1 (1983)
40. E.M. Levin, M.G. Ryskin, Y.M. Shabelsky, A.G. Shuvaev, Sov. J. Nucl. Phys. **53**, 657 (1991)
41. S. Catani, M. Ciafaloni, F. Hautmann, Nucl. Phys. B **366**, 135 (1991)
42. J.C. Collins, R.K. Ellis, Nucl. Phys. B **360**, 3 (1991)
43. E.A. Kuraev, L.N. Lipatov, V.S. Fadin, Sov. Phys. JETP **44**, 443 (1976)
44. E.A. Kuraev, L.N. Lipatov, V.S. Fadin, Sov. Phys. JETP **45**, 199 (1977)
45. I.I. Balitsky, L.N. Lipatov, Sov. J. Nucl. Phys. **28**, 822 (1978)
46. M. Ciafaloni, Nucl. Phys. B **296**, 49 (1988)
47. S. Catani, F. Fiorani, G. Marchesini, Phys. Lett. B **234**, 339 (1990)
48. S. Catani, F. Fiorani, G. Marchesini, Nucl. Phys. B **336**, 18 (1990)
49. G. Marchesini, Nucl. Phys. B **445**, 49 (1995)
50. R. Angeles-Martinez et al., Acta Phys. Polon. B **46**, 2501 (2015)
51. LHCb Collaboration, Eur. Phys. J. C **74**, 3092 (2014)
52. E. Bycling, K. Kajantie, *Particle Kinematics* (Wiley, New York, 1973)
53. C.-H. Chang, Nucl. Phys. B **172**, 425 (1980)
54. E.L. Berger, D.L. Jones, Phys. Rev. D **2**(3), 1521 (1981)
55. R. Baier, R. Rückl, Phys. Lett. B **102**, 364 (1981)
56. S.S. Gershtein, A.K. Likhoded, S.R. Slabospitsky, Sov. J. Nucl. Phys. **34**, 128 (1981)
57. A.V. Batunin, S.R. Slabospitsky, Phys. Lett. B **188**, 269 (1987)
58. P. Cho, M. Wise, S. Trivedi, Phys. Rev. D **51**, R2039 (1995)
59. H. Jung. arXiv:hep-ph/0411287
60. F. Hautmann, H. Jung, Nucl. Phys. B **883**, 1 (2014)
61. M.A. Kimber, A.D. Martin, M.G. Ryskin, Phys. Rev. D **63**, 114027 (2001)
62. A.D. Martin, M.G. Ryskin, G. Watt, Eur. Phys. J. C **31**, 73 (2003)
63. A.D. Martin, M.G. Ryskin, G. Watt, Eur. Phys. J. C **66**, 163 (2010)
64. NNPDF Collaboration, Eur. Phys. J. C **77**, 663 (2017)
65. F. Hautmann, H. Jung, A. Lelek, V. Radescu, R. Zlebcik, Phys. Lett. B **772**, 446 (2017)
66. F. Hautmann, H. Jung, A. Lelek, V. Radescu, R. Zlebcik, J. High Energy Phys. **01**, 070 (2018)
67. A.B. Martinez, P. Connor, H. Jung, A. Lelek, R. Zlebcik, F. Hautmann, V. Radescu, Phys. Rev. D **99**, 074008 (2019)
68. S.P. Baranov, A.V. Lipatov, M.A. Malyshev, Eur. Phys. J. C **80**, 4 (2020)
69. P.D.G. Collaboration, Phys. Rev. D **98**, 030001 (2018)
70. E.J. Eichten, C. Quigg. arXiv:1904.11542 [hep ph]
71. http://www.gnuplot.info/docs_5.2/Gnuplot_5.2.pdf
72. A.V. Lipatov, M.A. Malyshev, H. Jung, Phys. Rev. D **101**, 034022 (2020)
73. R. Maciula, A. Szczurek, Phys. Rev. D **100**, 054001 (2019)
74. F. Hautmann, L. Keersmaekers, A. Lelek, A.M. van Kampen, Nucl. Phys. B **949**, 114795 (2019)
75. CDF Collaboration, Phys. Rev. Lett. **88**, 161802 (2002)
76. M. Beneke, M. Krämer, M. Vänttinen, Phys. Rev. D **57**, 4258 (1998)